Influence of titanium dioxide surface activation on the performance of mesoscopic perovskite solar cells

Muhammad Talha Masood[a,b], Christian Weinberger[a], Syeda Qudsia[a], Emil Rosqvist[a], Oskar J. Sandberg[c], Mathias Nyman[c], Simon Sandén[c], Paola Vivo[d], Kerttu Aitola[e], Peter D. Lund[e], Ronald Österbacka[c], Jan-Henrik Smått[a,*]

[a] *Laboratory of Physical Chemistry, Faculty of Science and Engineering and Center for Functional Materials, Åbo Akademi University, Porthansgatan 3-5, 20500 Turku, Finland*
[b] *Department of Materials Engineering, School of Chemical & Materials Engineering, National University of Science & Technology (NUST), H-12 sector, Islamabad, Pakistan*
[c] *Laboratory of Physics, Faculty of Science and Engineering and Center for Functional Materials, Åbo Akademi University, Porthansgatan 3-5, 20500 Turku, Finland*
[d] *Laboratory of Chemistry and Bioengineering, Tampere University of Technology, P.O. Box 541, FI-33101 Tampere, Finland*
[e] *Department of Applied Physics, Aalto University, School of Science, P.O. Box 15100, FI-00076 Aalto, Finland*

ARTICLE INFO

Keywords:
Perovskite solar cells
Surface activation
Ultraviolet treatment
Plasma treatment
Lead iodide-to-perovskite conversion
Mesoscopic titanium dioxide scaffold

ABSTRACT

Perovskite solar cells with record efficiencies already above 24% are a highly promising clean energy technology. However, the reproducibility in their fabrication has proven to be challenging and needs more attention. Here we demonstrate that surface activation of the mesoscopic titanium dioxide (TiO_2) scaffold, utilized in the two-step perovskite synthesis process, significantly affects the final device performance. Irradiating the mesostructured substrate with ultraviolet (UV) light prior to lead iodide (PbI_2) deposition has a positive effect on the short-circuit current density and on the overall device performance (leading to a > 20% increase in efficiency in our devices). As most of the UV light is absorbed in the topmost TiO_2 layer, the interior of the scaffold remains less activated. This results in a sparsely packed PbI_2 structure that facilitates an efficient conversion to the perovskite, while the activated topmost surface improves the perovskite capping layer. On the contrary, plasma treatment of the scaffold also activates the interior parts of the scaffold, which leads to a dense PbI_2 structure that hampers the conversion and causing a > 25% efficiency drop. We show that also minor changes in the surface properties of the mesoporous TiO_2 scaffold can affect the device performance, which could explain some of the large efficiency variations observed between laboratories.

1. Introduction

With their skyrocketing efficiencies (above 24%) [1], strong light absorption, and unique charge transport characteristics, lead-based organohalide perovskite solar cells (PSCs) have proven to be strong candidates to challenge the conventional silicon-based solar cells [2]. However, before the PSC technology can reach a market breakthrough, issues related to reproducibility, scalability, and stability must be solved. Spawning from the dye-sensitized solar cell technology, the earliest PSC device configurations were utilizing a mesoscopic titanium dioxide (TiO_2) charge-selective layer, which also functioned as a scaffold for the perovskite crystallization [3,4]. However, when realized that the perovskite material could transport charges over extremely long distances virtually without recombination [5,6], also PSCs with planar (n-i-p type) device structures were developed [7]. Today, the best devices are hybrids of mesoscopic and planar device structures, i.e., they combine a thick perovskite capping layer with an underlying mesoscopic structure that facilitates the crystallization [8]. Nowadays also inverted (p-i-n type) device structures have shown excellent results as they offer the benefit of low-temperature processing and low current density – voltage (J-V) hysteresis [9–11]. Furthermore, fully printable carbon-based perovskite solar cells without hole-transport layers have shown great promise due to outstanding device stability [12,13].

Generally, the organohalide perovskite layer can be prepared with one-step or two-step approaches. In the one-step method, both the lead iodide (PbI_2) and methylammonium iodide (MAI) precursors are dissolved in a mutual solvent and deposited simultaneously, while the two-step approach takes advantage of a sequential deposition of the two

* Corresponding author.
E-mail address: jsmatt@abo.fi (J.-H. Smått).

precursors. Although it has some drawbacks, the combination of the two-step approach with a mesoscopic scaffold has proven to be a good method for making efficient devices [14]. In the two-step process, the porous scaffold allows the PbI_2 to crystallize in a more open structure, which is important in the second step when it is immersed in the MAI-containing solution [15]. If the PbI_2 layer is too dense, which is usually the case when a planar device configuration is used, the complete conversion to the perovskite is hampered as only the topmost part of the film is converted. Although the formation of pinholes in the perovskite layer in mesoscopic devices is not as common as in planar devices, they should be avoided in order not to cause surface recombination and shunts in the device. Thus, it is important that the scaffold material is completely covered by a capping layer of perovskite [14]. Increasing the wettability of the scaffold material is known to facilitate a better perovskite coverage as it generates more nucleation centers [16], and today ultraviolet (UV)-ozone treatment of oxide substrates is common practice (especially when using one-step perovskite synthesis protocols) to guarantee a good coverage of the perovskite layer and to remove residual organic molecules from the surface [17,18].

In order to illustrate that the surface activation procedure is even more crucial in the sequential perovskite deposition protocol, we have here studied the influence of UV and oxygen plasma activation of the mesoporous scaffold on the conversion efficiency of PbI_2 to the perovskite as well as on the device performance. As TiO_2 is photocatalytic, absorption of UV light can create highly reactive radicals, which can efficiently degrade nearby organic species [19], while oxygen/air plasma improves the wettability of oxide surfaces and efficiently oxidizes and removes contaminants [20]. Due to the deviating nature of these two activation procedures (UV activates only the topmost surface, while plasma activates the entire porous layer), the results we observed were also completely different. We show that activation of the topmost surface (by UV irradiation or by plasma cleaning) is beneficial for obtaining a uniform, pinhole-free perovskite capping layer, while activation inside the pore system (which is only achieved by plasma treatment) leads to a much lower PbI_2-to-perovskite conversion. Thus, in order to obtain devices with both good capping layers and high perovskite conversion, UV treatment of the mesoporous scaffold is the preferred method. It should also be noted that an activated (highly energetic) TiO_2 surface is very sensitive to volatile organic compounds and even in a few hours, the wettability of the TiO_2 surface might drastically change [21]. Thus, even small variations in the activation, handling, and storage procedures of the mesoscopic TiO_2 scaffold might explain the large deviations observed in device performance when using similar device fabrication protocols.

2. Materials and methods

2.1. Materials

Fluorine-doped tin oxide (FTO, TCO22–15) substrates were purchased from Solaronix, while titanium(IV) chloride ($TiCl_4$, > 99%) was bought from Fluka. Chemicals purchased from Sigma-Aldrich include Pluronic F127 block *co*-polymer, *N*,*N*-dimethylformamide (DMF, 99.8%), 2-propanol (99.5%), chlorobenzene (99.8%), acetonitrile (99.8%), bis(trifluoromethane)sulfonimide lithium salt (Li-TFSI), tetrahydrofuran (THF, > 99%). The PbI_2 (99.99%) and MAI (> 98%) were purchased from TCI Europe, spiro-OMeTAD from Feiming Chemicals Ltd., while cobalt (III) tri[bis-(trifluromethane]sulfonamide) (FK209 Cobalt (III) salt) and 30 NR-D TiO_2 paste were obtained from Dyesol. Ethanol (EtOH, > 99.5%) was bought from ALTIA Plc, Finland.

2.2. Compact and mesoporous TiO_2 layers

The compact TiO_2 (c-TiO_2) dip coating solution was prepared as described earlier by Masood et al. [22]. Initially, a $TiCl_4$:EtOH stock solution was prepared by adding 18.97 g of $TiCl_4$ dropwise into 23.04 g of EtOH while stirring in an ice bath. Another solution was prepared by mixing 0.0152 g of F127 block *co*-polymer, 12.34 g of EtOH, 0.21 g of deionized water and 1.717 g of THF. Then, 2.50 g of the first $TiCl_4$:EtOH stock solution was added dropwise into the second solution and stirred for 30 min before dip coating the solution onto the FTO substrates. FTO substrates cut into 4 cm × 2 cm pieces were sonicated in 2% aqueous solution of Hellmanex III detergent, deionized water, acetone and isopropanol for 10min each and then dried with dry nitrogen. The substrates were plasma-treated for 5 min each and then dip-coated with the c-TiO_2 solution using a withdrawal speed of 85 mm/min. The coated substrates were then dried on a hot plate at 125°C and finally calcined directly at 500 °C for 30 min in air. Thereafter, a suspension of TiO_2 nanoparticles (0.15 g/mL of 30 NR-D TiO_2 paste diluted in EtOH) was spin-coated at 4000 rpm for 10s (acceleration of 2000 rpm/s) on top of the c-TiO_2/FTO substrates. After the deposition of the mesoporous layer, the films were calcined at 450°C for 30 min using the following heating ramp:

$$\xrightarrow{20^{\circ}C/min} 125^{\circ}C\ (5\ \text{min}) \xrightarrow{13.3^{\circ}C/min} 325^{\circ}C\ (5\ \text{min}) \xrightarrow{10^{\circ}C/min} 375^{\circ}C\ (5\ \text{min}) \xrightarrow{15^{\circ}C/min} 450^{\circ}C\ (30\ \text{min})$$

2.3. Surface activation of the substrates

After calcination, some of the samples were immediately transferred to a nitrogen-containing glovebox without any surface activation (denoted: non-treated), while the rest of the coated substrates were activated either by UV light or plasma treatment. In the UV treatment (denoted: UV-treated), the substrates were exposed to UV light for 20min in air (relative humidity ~20%) using a Mineralight UVS-11E UV lamp with λ_{max} at 254 nm. The plasma activation (denoted: plasma-treated) was performed for 5 min under low air pressure using a Harrick PDC-32G plasma cleaner. Thereafter, these samples were also transferred to the glovebox, after which the rest of the processing was done in a dry nitrogen atmosphere.

2.4. Perovskite deposition

A 1 M solution of PbI_2 was prepared in anhydrous DMF at 100 °C and kept at the same temperature throughout the experiment to avoid any precipitation of PbI_2 crystals in the solution. The PbI_2 solution was spin-coated on all substrates with a spin speed of 6000 rpm for 30 s using a 6100 rpm/s acceleration rate. The substrates were then dried on a hot plate at 100 °C for 30 min. The PbI_2-coated substrates were dipped for 1 min in 10 mg/mL of MAI dissolved in anhydrous isopropanol followed by rinsing in anhydrous isopropanol to get rid of excess MAI crystals on the surface. These substrates were then dried again on a hot plate at 100 °C for 30 min.

2.5. Characterization methods

Grazing incidence x-ray diffraction (GI-XRD) was performed on the perovskite films (i.e., perovskite/TiO_2 composite films on top of c-TiO_2/FTO substrates) using a Bruker AXS D8 Discover instrument. The 2θ scan was performed between 10° to 20° with a step size of 0.04°, and grazing incidence angles of 0.5°, 1° and 2°. UV–visible (UV–vis) absorption of the thin films was measured using a Perkin Elmer Lambda 900 UV–vis/near infrared spectrometer. The scan range was kept between 300 nm to 900 nm, and the measurement was performed in the presence of certified reflectance standards. The slit size was 2 mm. Field emission scanning electron microscopy (FE-SEM) was performed on PbI_2 and perovskite samples to evaluate the morphology of the capping layer using a magnification of 50 k times, electron high tension of 2.70 kV, and an aperture size of 10 μm. Water contact angle measurements were carried out using a CAM-200 goniometer from KSV instruments Ltd. In order to study the effectiveness of the different surface

activation methods, mp-TiO_2 films were infiltrated with a model dye (N719 from Solaronix, 3mM in EtOH). UV–vis measurements were done on the same substrates before and after dye loading as well as after UV or plasma activation.

2.6. Device fabrication

Devices using the same surface activation protocols were also fabricated using an earlier protocol [22]. A 1.5 cm × 2 cm area from one side of the 4 cm × 2 cm-sized FTO substrates was etched with Zn powder and 4 M HCl solution in water. Compact TiO_2, mesoporous TiO_2, and the perovskite layers were deposited as mentioned above. We fabricated 4–6 devices for each of the different mp-TiO_2 surface activation methods. Once the perovskite films were ready, spiroOMeTAD and 4-tertbutyilpyridine were dissolved in chlorobenzene. Solutions of lithium bis(trifluoromethylsulfonyl)imide and FK209 Co(III) dissolved in acetonitrile were added to the solution of spiroOMeTAD to maintain the molar ratio of 1.0: 0.5: 2.5×10^{-2}: 3.3: 131.5: 7.2 (spiroOMeTAD: Li-TFSI: FK209 Co (III): 4-tertbutylpuridine: chlorobenzene: acetonitrile). The final solution was then spin-coated on top of the perovskite layer at a spin speed of 4000 rpm for 30 s using 4000 rpm/s spin acceleration. Circular gold metal back contacts (area: 0.283cm^2) were deposited by evaporating gold at an evaporation rate of about 0.01 nm/s with a vacuum pressure of about 2×10^{-5} mbar.

2.7. Device characterization

J-V curves were measured in ambient conditions under illumination using simulated AM 1.5 sunlight with an Oriel Class ABB solar simulator, 150 W, 2″ × 2″. The devices were masked, and the aperture size was kept at 0.126 cm^2. The voltage scan was performed from −0.3 V to 1.1 V in forward sweep and then from 1.1 V to −0.3 V in reverse sweep using a scan speed of 10 mV s^{-1} [23,24]. For each surface treatment series, 4–6 devices were characterized to determine the photovoltaic parameters. The hysteresis index was calculated according to the method described by Nemnes et al. [25].

3. Results and discussion

3.1. Characterization of the PbI_2 and perovskite layers

Initially, we investigated how the various surface treatments of the mp-TiO_2 layer affect the formation of the PbI_2 layer as well as how the subsequent conversion to the perovskite is affected. From the XRD plots in Fig. 1, it is evident that all samples contain both PbI_2 and perovskite phases after reaction in MAI solution, as the reflections at about 12.6° and 14.1° typically are associated with the (001) reflection of PbI_2 and the (110) reflection of methylammonium lead iodide ($MAPbI_3$) phases, respectively. From the peak areas of these reflections (Table 1), we can estimate and compare how efficiently the PbI_2 has been converted to $MAPbI_3$ as a function of the various surface treatments and grazing incidence angles. A higher area percentage of the perovskite reflection indicates a better conversion. The non-activated sample gives a perovskite peak area of 68.8% (at a GI angle of 1°), which is comparable to what has been observed previously by Murugadoss et al. [26]. The UV-activated and plasma-activated samples give perovskite peak areas of 65.7% and 38.1%, respectively. This suggests that the PbI_2-to-perovskite conversion is slightly lower for the UV-treated sample, while it is much more suppressed by the plasma treatment. As the original amount of PbI_2 can be assumed the same in all samples, a better conversion would generate more perovskite in absolute amounts. Furthermore, grazing incidence angle-dependent XRD measurements suggest that the conversion to perovskite is more efficient closer to the surface of the films, as the lowest GI angle (0.5°) shows the highest PbI_2-to-perovskite conversion for all samples.

From the UV–vis data in Fig. 2 and Table 1, typical absorbance

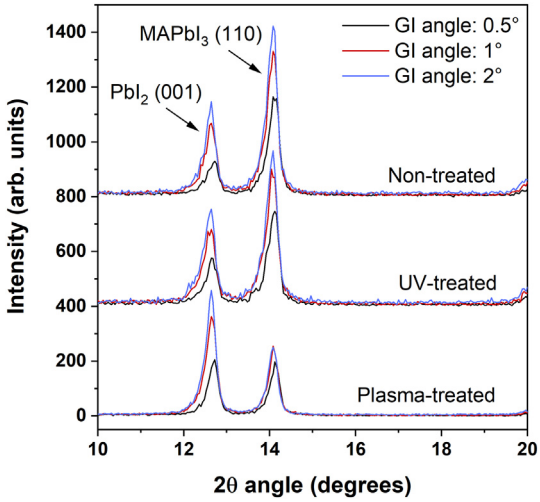

Fig. 1. XRD patterns for the perovskite films prepared on top of mesoporous TiO_2 scaffolds activated by various methods at different grazing incidence angles.

Table 1
GI-XRD results indicating the relative perovskite content at different grazing incidence angles as well as UV–vis transmittance values.

Sample	Perovskite peak area at different GI angles			Transmittance at 700 nm
	0.5°	1°	2°	
Non-treated	77.2%	68.8%	67.9%	38.6%
UV-treated	67.5%	65.7%	61.5%	38.1%
Plasma-treated	48.3%	38.1%	34.3%	46.1%

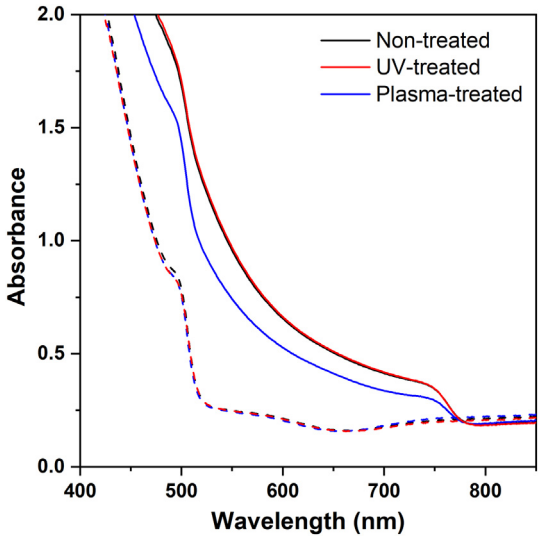

Fig. 2. UV–vis absorption spectra for PbI_2 films (dashed lines) and perovskite films (solid lines) deposited on mp-TiO_2 films with different surface treatments.

spectra of perovskite-containing films with the characteristic absorption in the 500–750 nm wavelength range can be discerned. The UV-activated sample shows a similar absorption in this range (38.1% transmittance at 700 nm) as the non-activated sample (38.6% transmittance). On the other hand, the plasma-treated sample shows the lowest absorbance in this range (46.1% transmittance at 700 nm). Thus, we can conclude that the amount of perovskite is the highest for the non-treated and UV-treated samples and lowest for the plasma-treated sample, which follows the same trend as observed in the XRD data.

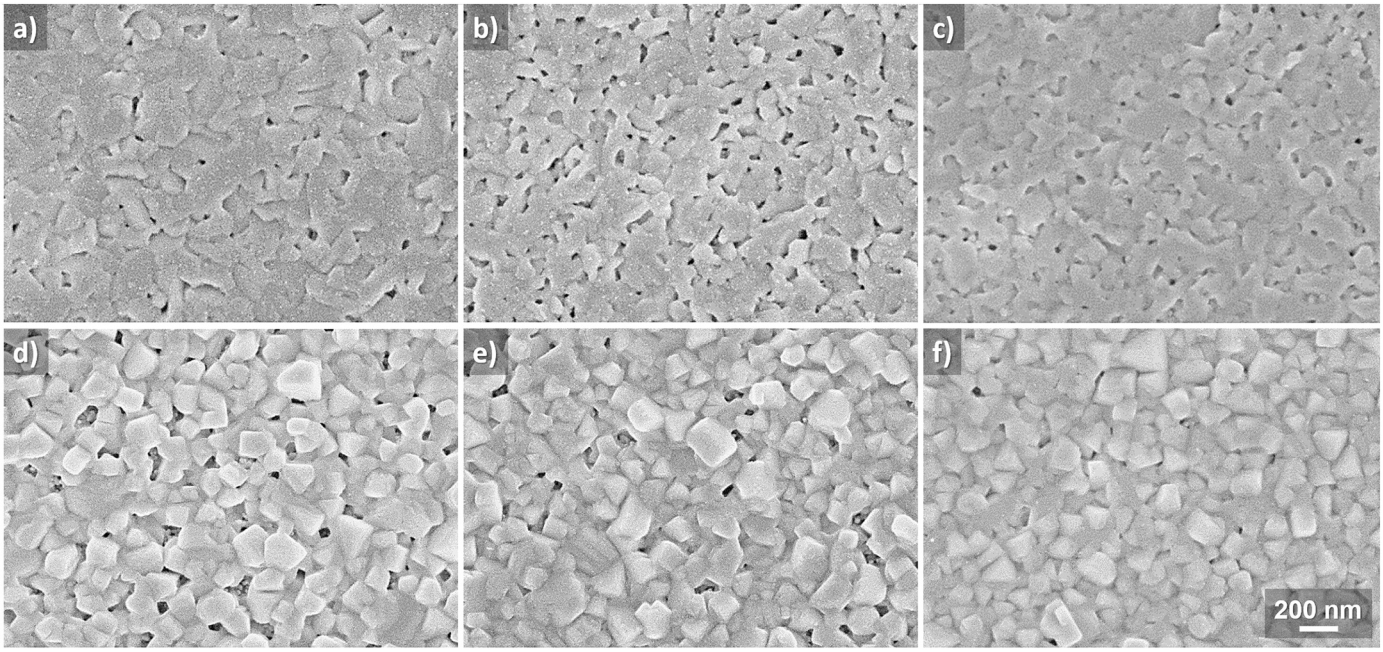

Fig. 3. Representative SEM images of the PbI_2 capping layers deposited on mp-TiO_2 activated by different methods: a) non-treated, b) UV-treated, and c) plasma-treated. The corresponding perovskite capping layers after conversion are shown in d), e), and f).

Finally, the UV–vis spectra of the unconverted PbI_2 films shows that the different activation methods do not alter the amounts of PbI_2.

Top-view SEM characterization was used to further study how the different surface activation protocols affect the PbI_2 and perovskite capping layers. Starting from the PbI_2 films (Fig. 3a–c), we can see that the mp-TiO_2 films are covered with moderately open capping layers. However, from the SEM images, we are not able to investigate the PbI_2 structures inside the pores. Although the openness of the PbI_2 capping layer might be beneficial, we do not think this is decisive for the perovskite conversion efficiency. This should be more related to the denseness of the PbI_2 inside the pore structure. After the films have been further processed in the MAI solution, we can also see that the resulting perovskite capping layers contain some pinholes in the crystalline structure (Fig. 3d–f). Importantly, the number of pinholes seems to decrease when going from the non-treated sample to the UV-treated sample and finally to the plasma-treated sample. As will be discussed later, this will also influence the device performance (especially the open circuit voltage, V_{OC}).

3.2. Device characterization

Fig. 4 shows J–V curves of representative samples from each series, while the mean photovoltaic parameters for 4–6 devices per type are summarized in Table 2. The devices made from mp-TiO_2 without any additional surface activation step show good photovoltaic behavior with a short-circuit current density (J_{SC}) of about 13.7 mA/cm^2, a V_{OC} of 0.91 V, and a fill factor (FF) of 0.62 in the forward bias. This results in a power conversion efficiency (PCE) of 7.6%, which is slightly below the efficiencies observed earlier [14,22]. The reason for this may lie in slightly thinner PbI_2 and mp-TiO_2 layers, a relatively large cell area, or a lower conversion of PbI_2 to perovskite. Furthermore, all the J-V curves display low hysteresis (hysteresis indices below 1%), which was also observed in our earlier studies [22].

Rather surprisingly, the overall efficiency improves drastically up to 9.3% for the UV-treated sample, which represents an increase by > 20% compared to the samples without activation. On the other hand, the plasma-treated samples show an overall worse performance; PCE = 5.6%, which is < 75% of the efficiency of the non-treated reference devices. These results highlight the importance of the surface

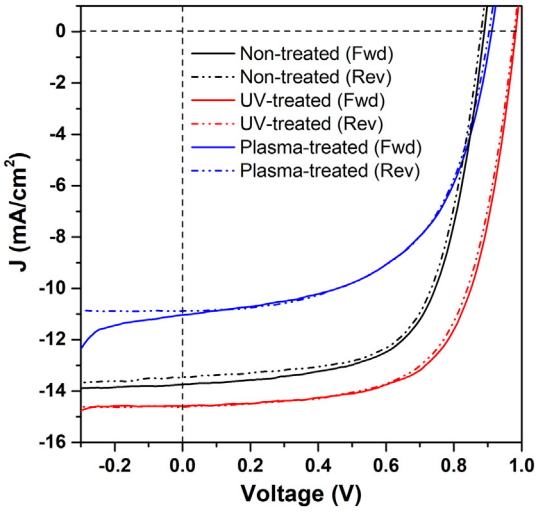

Fig. 4. J-V curves under illumination for representative devices prepared after applying different surface treatments to the TiO_2 scaffold.

Table 2
Average photovoltaic parameters and standard deviation (n = 4–6) for each type of devices.

	J_{SC} (mA/cm^2)	V_{OC} (V)	FF	PCE (%)
Forward sweep				
Non-treated	13.7 ± 0.3	0.91 ± 0.02	0.62 ± 0.02	7.6 ± 0.3
UV-treated	14.4 ± 0.3	0.96 ± 0.02	0.66 ± 0.01	9.3 ± 0.3
Plasma-treated	10.8 ± 1.0	0.91 ± 0.02	0.57 ± 0.02	5.6 ± 0.5
Reverse sweep				
Non-treated	13.3 ± 0.4	0.90 ± 0.03	0.62 ± 0.02	7.4 ± 0.3
UV-treated	14.4 ± 0.3	0.96 ± 0.02	0.65 ± 0.02	9.0 ± 0.4
Plasma-treated	10.7 ± 0.9	0.87 ± 0.08	0.55 ± 0.08	5.2 ± 1.2

activation, as the PCE can vary from 5.6% to 9.3% by just applying different mp-TiO_2 surface activation protocols. When comparing the J_{SC} values, it is evident that they correlate well with the total amount of perovskite in the device observed in the XRD and UV–vis measurements (Figs. 1 and 2, respectively). As the plasma-treated sample has the lowest fraction of perovskite, it also has the lowest light absorption capacity and charge generation in the device. Thus, a more complete conversion from PbI_2 to perovskite will lead to a higher J_{SC} and a better overall device performance, which is the case for the non-treated and UV-treated samples. The slight improvement in the J_{SC} for the UV-treated sample could be explained by less charge recombination as a result of a reduced number of pinholes in the perovskite capping layer. Additionally, differences in the area fraction of pinholes in the perovskite capping layer can also explain shifts in the V_{OC} and FF [27]. If the capping layer does not fully cover the mp-TiO_2 layer, shunt paths between the spiroOMeTAD and TiO_2 layers will cause a decrease in the V_{OC} and fill factor. Thus, the relatively large V_{OC} for the plasma-treated sample can partially be explained by the smaller number of pinholes seen in the SEM image in Fig. 3.

3.3. Proposed formation mechanism

The large variations in the results discussed above illustrate the importance of a careful control of the processing conditions. Particularly, the wettability of the PbI_2 and perovskite layers on the substrate material has a pivotal role on the final perovskite structure. The wettability of the substrate can be easily controlled by the type of surface activation method used and we propose the following formation mechanisms of the different cases, which is illustrated in Fig. 5.

It is expected that the UV treatment only activates the topmost fraction of the ~150 nm thick mesoporous TiO_2 film. Wahl and Augustynski estimated that the penetration depth of UV light (λ = 300 nm) is approximately 30 nm for a similar porous TiO_2 film [28]. However, the charges generated in this layer can potentially diffuse throughout this layer and create reactive surface groups deeper in the films. Thus, a gradually decreasing activation level deeper in the film is probably a more realistic estimation. On the other hand, the plasma treatment is also activating the interior part of the porous structure. We investigated this further using time-dependent water contact angle measurements and dye degradation studies (Figs. 6 and 7). The non-treated sample is wetted by water fairly well, with a contact angle close to 9°. One has to keep in mind that the wettability of a surface is strongly roughness dependent, which could potentially make a porous surface more hydrophilic than a flat surface of similar chemistry [20]. Nonetheless, after UV activation for 20min, a contact angle of zero degrees (i.e., complete wetting) is reached within 0.6 s after applying the water droplet. This indicates that possible organic contaminants have been removed from at least the topmost layer of the porous films. After plasma activation, a similar time-dependence of the droplet spreading can be seen. Other research groups have previously observed comparable results for UV- and plasma-activated TiO_2 thin films [20,29]. Unfortunately, from our results, we cannot deduce whether the interior of the pore structure has been activated or not (or to which degree it has been activated). Nonetheless, from the dye degradation results shown in Fig. 7, it is evident that the plasma treatment can degrade almost all of the model dye N719 dye, while the UV treatment only removes a small fraction of the dye molecules. In

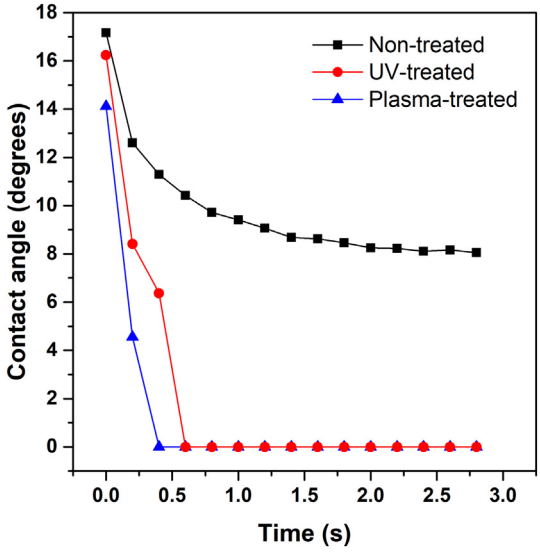

Fig. 6. Water contact angle measurements of different surface-treated mesoporous TiO_2 substrates on c-TiO_2/FTO substrates.

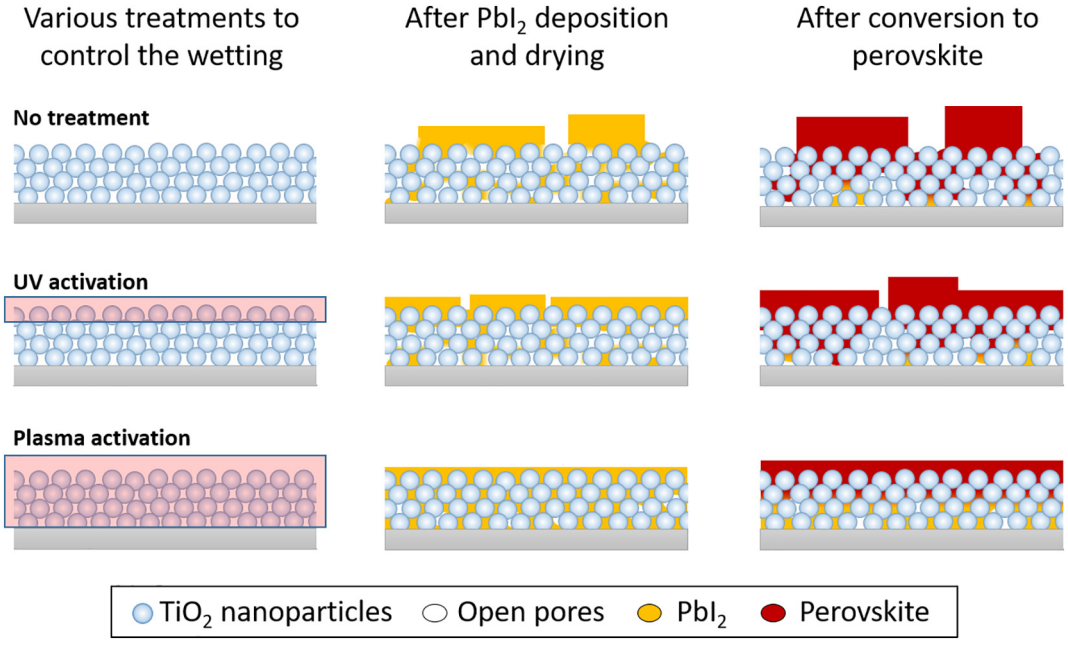

Fig. 5. Proposed PbI_2 and perovskite formation mechanisms as a function of surface activation method.

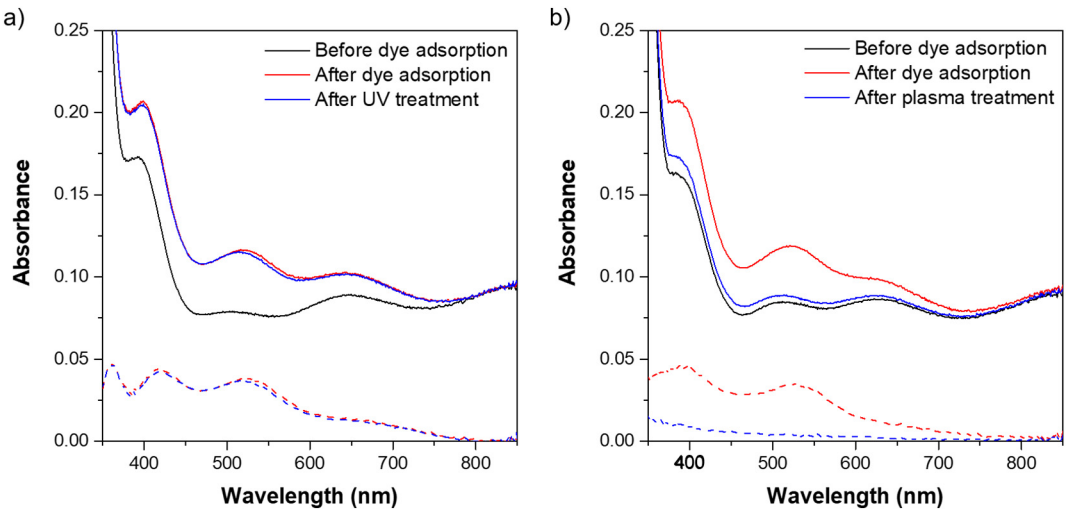

Fig. 7. UV–vis spectra of the same films before and after adsorption of N719 dye as well as after surface activation with a) UV light and b) plasma. The dashed lines represent the absorption spectra where the non-dyed substrates have been subtracted.

combination with the water contact angle measurements, this means we can conclude that the plasma activation has a deeper penetration depth in porous films compared to simple UV treatments.

An improved wettability of the interior of the porous structure (which is expected in the case of the plasma-activated sample), would lead to a better infiltration of the pores with the PbI_2 salt (as illustrated in Fig. 5). Unfortunately, the dense packing of the PbI_2 inside the pores also makes the conversion to the perovskite more difficult due to the inaccessibility to the bottom parts of the films as well as the blocking of the pore entrances due to the large volume expansion associated with the conversion of PbI_2 to $MAPbI_3$ [30]. On the other hand, the packing of the PbI_2 salt inside both the non-activated and UV-activated samples would be less dense, and pathways are open down to the bottom of the films, which facilitates a more complete conversion to the perovskite. This is directly evidenced in the XRD, UV–vis and J-V data (higher photocurrent densities) as previously discussed. Similar improvements have also been observed when the thickness and porosity of the mesoporous layer was changed or when the PbI_2 loading amount was altered [14,26,31]. However, this does not explain why the UV-treated sample behaves much better than the non-treated sample. The activation of the topmost layer of the porous scaffold is important for obtaining a pinhole-free capping layer of the perovskite. Without any activation, poor wettability allows for the formation of a large number of pinholes in the capping layer. However, both with UV and plasma treatments the spreading (and nucleation) of the perovskite on the topmost surface is clearly improved. Furthermore, the reduction in the number of pinholes leads to an increase in the V_{OC} of the device (i.e., lower shunt resistance and/or surface recombination) [32]. Thus, as the UV treatment only activates the topmost fraction of the film, it allows for both a good conversion to the perovskite as well as a good capping layer with a small number of pinholes. Other studies on inverted organic solar cells have shown that UV exposure also can lower the work function at the indium tin oxide/TiO_2 contact and in that way improve the performance of the device [33]. However, we note that in our case, the films were exposed to the UV light only from the mp-TiO_2 side, which should absorb most of the photons in the UV range. More generally, these results imply that the pretreatment of the mesoscopic TiO_2 scaffold plays an immense role in the device fabrication of PSCs. It is very important to carefully consider how to activate and store the mesoporous scaffold prior to PbI_2 deposition (including the storage duration). This could be the reason for the vast reproducibility issues reported between different labs and could even explain variations observed within the same lab.

4. Conclusions

In this study, we have demonstrated that the type of surface activation method significantly affects the device performance of mesoscopic perovskite solar cells produced by the two-step deposition method. Although both UV and plasma treatments clearly improved the wettability of the topmost surface of mesoscopic TiO_2 films, our dye degradation tests revealed that the penetration depth of the different activation methods was very diverse. While plasma activation for 5 min efficiently removed organic contaminants from the entire scaffold, UV irradiation ($\lambda = 254$ nm) for 20 min only activated the topmost layer of the films. Because of the enhanced wettability inside the mesoporous scaffold, a denser PbI_2 structure was formed inside the plasma-activated substrate. Consequently, this had a hampering effect on the perovskite conversion when the sample was subsequently immersed in the MAI solution. On the contrary, the UV activation did not have a negative effect on the PbI_2-to-perovskite conversion, but still benefitted from the improved perovskite capping layer due to the better wettability of the topmost mp-TiO_2 layer. When assembled into devices, PSCs made from the plasma-treated scaffolds displayed a much lower J_{SC} compared to the non-treated samples, while the J_{SC} was clearly improved for samples made from UV-treated scaffolds. These large deviances in J_{SC} could be explained by the differences in PbI_2-to-perovskite conversion efficiency and charge recombination. Furthermore, also the V_{OC} increased (from about 0.91 V to 0.96 V) when the substrate had been irradiated with UV light, and we ascribe this effect to an improved perovskite capping layer with reduced number of pinholes. Although these findings clearly illustrate the potential problems that can arise if the processing parameters are not carefully controlled, they also underline the importance for further research to optimize the many parameters involved, including other activation methods (e.g., UV-ozone), different treatment times, various storage and handling conditions, to name just a few.

Acknowledgements

The Academy of Finland (grant no. 308307) and Jane and Aatos Erkko Foundation (grant no. 3448-94643) are greatly acknowledged for financial support. C.W. thanks the Deutsche Forschungsgemeinschaft (DFG, WE 6127/1-1) for a Postdoctoral Fellowship.

References

[1] Best Research Cell-Efficiencies, National Renewable Energy Laboratory (NREL), https://www.nrel.gov/pv/cell-efficiency.html, (May 28 2019).

[2] H.J. Snaith, Present status and future prospects of perovskite photovoltaics, Nat. Mater. 17 (2018) 372–376, https://doi.org/10.1038/s41563-018-0071-z.

[3] A. Kojima, K. Teshima, Y. Shirai, T. Miyasaka, Organometal halide perovskites as visible-light sensitizers for photovoltaic cells, ACS Commun. 131 (2009) 6050–6051, https://doi.org/10.1021/ja809598r.

[4] M.M. Lee, J. Teuscher, T. Miyasaka, T.N. Murakami, H.J. Snaith, Efficient hybrid solar cells based on meso-superstructured organometal halide perovskites, Science 338 (2012) 643–647, https://doi.org/10.1126/science.1228604.

[5] S.D. Stranks, G.E. Eperon, G. Grancini, C. Menelaou, M.J.P. Alcocer, T. Leijtens, L.M. Herz, A. Petrozza, H.J. Snaith, Electron-hole diffusion lengths exceeding 1 micrometer in an organometal trihalide perovskite absorber, Science 342 (2013) 341–344, https://doi.org/10.1126/science.1243982.

[6] G. Xing, N. Mathews, S. Sun, S.S. Lim, Y.M. Lam, M. Grätzel, S. Mhaisalkar, T.C. Sum, Long-range balanced electron- and hole-transport lengths in organic-inorganic $CH_3NH_3PbI_3$, Science 342 (2013) 344–347, https://doi.org/10.1126/science.1243167.

[7] M. Liu, M.B. Johnston, H.J. Snaith, Efficient planar heterojunction perovskite solar cells by vapour deposition, Nature 501 (2013) 395–398, https://doi.org/10.1038/nature12509.

[8] M. Saliba, T. Matsui, J.Y. Seo, K. Domanski, J.P. Correa-Baena, M.K. Nazeeruddin, S.M. Zakeeruddin, W. Tress, A. Abate, A. Hagfeldtd, M. Grätzel, Cesium-containing triple cation perovskite solar cells: improved stability, reproducibility and high efficiency, Energy Environ. Sci. 9 (2016) 1989–1997, https://doi.org/10.1039/C5EE03874J.

[9] R. Chen, T. Bu, J. Li, W. Li, P. Zhou, X. Liu, Z. Ku, J. Zhong, Y. Peng, F. Huang, Y.B. Cheng, Z. Fu, Efficient and stable inverted planar perovskite solar cells using a triphenylamine hole-transporting material, ChemSusChem 11 (2018) 1467–1473, https://doi.org/10.1002/cssc.201800476.

[10] M. Jahandar, N. Khan, H.K. Lee, S.K. Lee, W.S. Shin, J.C. Lee, C.E. Song, S.J. Moon, High-performance $CH_3NH_3PbI_3$-inverted planar perovskite solar cells with fill factor over 83% via excess organic/inorganic halide, ACS Appl. Mater. Interfaces 9 (2017) 35871–35879, https://doi.org/10.1021/acsami.7b11083.

[11] W. Chen, F.Z. Liu, X.Y. Feng, A.B. Djurišić, W.K. Chan, Z.B. He, Cesium doped NiOx as an efficient hole extraction layer for inverted planar perovskite solar cells, Adv. Energy Mater. 7 (2017) 1700722, , https://doi.org/10.1002/aenm.201700722.

[12] A. Mei, X. Li, L. Liu, Z. Ku, T. Liu, Y. Rong, M. Xu, M. Hu, J. Chen, Y. Yang, M. Grätzel, H. Han, A hole-conductor-free, fully printable mesoscopic perovskite solar cell with high stability, Science 345 (2014) 295–298, https://doi.org/10.1126/science.1254763.

[13] X. Meng, J. Zhou, J. Hou, X. Tao, S.H. Cheung, S.K. So, S. Yang, Versatility of carbon enables all carbon based perovskite solar cells to achieve high efficiency and high stability, Adv. Mater. 30 (2018) 1706975, , https://doi.org/10.1002/adma.201706975.

[14] J. Burschka, N. Pellet, S.J. Moon, R. Humphry-Baker, P. Gao, M.K. Nazeeruddin, M. Grätzel, Sequential deposition as a route to high-performance perovskite-sensitized solar cells, Nature 499 (2013) 316–320, https://doi.org/10.1038/nature12340.

[15] A. Ummadisingu, M. Grätzel, Revealing the detailed path of sequential deposition for metal halide perovskite formation, Sci. Adv. 4 (2018) e1701402, , https://doi.org/10.1126/sciadv.1701402.

[16] F. Huang, A.R. Pascoe, W.Q. Wu, Z. Ku, Y. Peng, J. Zhong, R.A. Caruso, Y.B. Cheng, Effect of the microstructure of the functional layers on the efficiency of perovskite solar cells, Adv. Mater. 29 (2017) 1601715, , https://doi.org/10.1002/adma.201601715.

[17] Z. Wang, J. Fang, Y. Mi, X. Zhu, H. Ren, X. Liu, Y. Yan, Enhanced performance of perovskite solar cells by ultraviolet-ozone treatment of mesoporous TiO_2, Appl. Surf. Sci. 436 (2018) 596–602, https://doi.org/10.1016/j.apsusc.2017.12.085.

[18] L. Cojocaru, S. Uchida, P.V.V. Jayaweera, S. Kaneko, H. Wang, J. Nakazaki, T. Kubo, H. Segawa, Effect of TiO_2 surface treatment on the current–voltage hysteresis of planar-structure perovskite solar cells prepared on rough and flat fluorine-doped tin oxide substrates, Energy Technol. 5 (2017) 1762–1766, https://doi.org/10.1002/ente.201700664.

[19] A. Carretero-Genevrier, C. Boissiere, L. Nicole, D. Grosso, Distance dependence of the photocatalytic efficiency of TiO_2 revealed by in situ ellipsometry, J. Am. Chem. Soc. 134 (2012) 10761–10764, https://doi.org/10.1021/ja303170h.

[20] T.A. Otitoju, A.L. Ahmad, B.S. Ooi, Superhydrophilic (superwetting) surfaces: a review on fabrication and application, J. Ind. Eng. Chem. 47 (2017) 19–40, https://doi.org/10.1016/j.jiec.2016.12.016.

[21] A. Kanta, R. Sedev, J. Ralston, Thermally- and photoinduced changes in the water wettability of low-surface-area silica and titania, Langmuir 21 (2005) 2400–2407, https://doi.org/10.1021/la047721m.

[22] M.T. Masood, C. Weinberger, J. Sarfraz, E. Rosqvist, S. Sandén, O.J. Sandberg, P. Vivo, G. Hashmi, P.D. Lund, R. Österbacka, J.H. Smått, Impact of film thickness of ultra-thin dip-coated compact TiO_2 layers on the performance of mesoscopic perovskite solar cells, ACS Appl. Mater. Interfaces 9 (2017) 17906–17913, https://doi.org/10.1021/acsami.7b02868.

[23] M. Saliba, J.P. Correa-Baena, C.M. Wolff, M. Stolterfoht, N. Phung, S. Albrecht, D. Neher, A. Abate, How to make over 20% efficient perovskite solar cells in regular (n−i−p) and inverted (p−i−n) architectures, Chem. Mater. 30 (2018) 4193–4201, https://doi.org/10.1021/acs.chemmater.8b00136.

[24] J.P. Correa-Baena, A. Abate, M. Saliba, W. Tress, T.J. Jacobsson, M. Grätzel, A. Hagfeldt, The rapid evolution of highly efficient perovskite solar cells, Energy Environ. Sci. 10 (2017) 710–727, https://doi.org/10.1039/C6EE03397K.

[25] G.A. Nemnes, C. Besleaga, A.G. Tomulescu, A. Palici, L. Pintilie, A. Manolescu, I. Pintilie, How measurement protocols influence the dynamic J-V characteristics of perovskite solar cells: theory and experiment, Sol. Energy 173 (2018) 976–983, https://doi.org/10.1016/j.solener.2018.08.033.

[26] G. Murugadoss, G. Mizuta, S. Tanaka, H. Nishino, T. Umeyama, H. Imahori, S. Ito, Double functions of porous TiO_2 electrodes on $CH_3NH_3PbI_3$ perovskite solar cells: enhancement of perovskite crystal transformation and prohibition of short circuiting, APL Mater. 2 (2014) 081511, , https://doi.org/10.1063/1.4891597.

[27] G.E. Eperon, V.M. Burlakov, P. Docampo, A. Goriely, H.J. Snaith, Morphological control for high performance, solution-processed planar heterojunction perovskite solar cells, Adv. Funct. Mater. 24 (2014) 151–157, https://doi.org/10.1002/adfm.201302090.

[28] A. Wahl, J. Augustynski, Charge carrier transport in nanostructured anatase TiO_2 films assisted by the self-doping of nanoparticles, J. Phys. Chem. B 102 (1998) 7820–7828, https://doi.org/10.1021/jp9814000.

[29] N. Ishida, D. Fujita, Superhydrophilic TiO_2 surfaces generated by reactive oxygen treatment, J. Vac. Sci. Technol. A 30 (2012) 051402, , https://doi.org/10.1116/1.4736946.

[30] X. Cao, L. Zhi, Y. Li, F. Fang, X. Cui, Y. Yao, L. Ci, K. Ding, J. Wei, Control of the morphology of PbI_2 films for efficient perovskite solar cells by strong Lewis base additives, J. Mater. Chem. C 5 (2017) 7458–7464, https://doi.org/10.1039/C7TC01973D.

[31] X. Sun, J. Xu, L. Xiao, J. Chen, B. Zhang, J. Yao, S. Dai, Influence of the porosity of the TiO_2 film on the performance of the perovskite solar cell, Int. J. Photoenergy (2017) 4935265, , https://doi.org/10.1155/2017/4935265.

[32] O.J. Sandberg, A. Sundqvist, M. Nyman, R. Österbacka, Relating charge transport, contact properties, and recombination to open-circuit voltage in sandwich-type thin-film solar cells, Phys. Rev. Appl. 5 (2016) 044005, , https://doi.org/10.1103/PhysRevApplied.5.044005.

[33] A. Sundqvist, O.J. Sandberg, M. Nyman, J.H. Smått, R. Österbacka, Origin of the s-shaped JV curve and the light-soaking issue in inverted organic solar cells, Adv. Energy Mater. 6 (2016) 1502265, , https://doi.org/10.1002/aenm.201502265.